International Journal of Engineering and Technology Innovation, vol. 14, no. 4, 2024, pp. 423-433

Self-Sensing Potential of Metashale Geopolymer Mortars with Carbon Fiber/Graphite Powder Admixtures

Petr Hotěk[1,*], Jiří Litoš[2], Wei-Ting Lin[3], Lukáš Fiala[1]

[1]Department of Materials Engineering and Chemistry, Faculty of Civil Engineering, Czech Technical University in Prague, Prague, Czech Republic

[2]Experimental Centre, Faculty of Civil Engineering, Czech Technical University in Prague, Prague, Czech Republic

[3]Department of Civil Engineering, National Ilan University, Yilan, Taiwan, ROC

Received 12 April 2024; received in revised form 28 May 2024; accepted 29 May 2024

DOI: https://doi.org/10.46604/ijeti.2024.13570

Abstract

Multifunctional building materials with self-sensing capability have great potential for civil engineering applications. The self-sensing capability of typically calcium aluminosilicate matrices of cementitious or geopolymer materials is adopted by admixing electrically conductive admixtures in an amount that ensures optimal electrical properties and their proportionality to mechanical loading. The paper aims to evaluate the self-sensing capability of 4 metashale geopolymer mortars with graphite powder (GP) and carbon fibers (CF) in different ratios, including MGF 5/0, MGF 4.5/0.5, MGF 4/1, and MGF 3/0. The 4-probe measurements at 21 V DC input voltage on (100 × 100 × 100) mm^3 samples with embedded copper-grid electrodes evaluate the gauge factor, which corresponds to the monitored changes in electrical resistivity. Despite the limitations of DC measurements, the self-sensing capability is observed for all the mixtures. The most promising response to dynamic loading with an FCR of 0.018%, is observed for the MGF 4.5/0.5 sample.

Keywords: geopolymers, self-sensing, carbon fibers, graphite powder, DC

1. Introduction

In recent years, multiple reconstructions and massive construction of urban infrastructure were realized to improve the living standards of the population. This process was accompanied by high consumption of raw construction materials and products. The most widely used building material is concrete, which corresponds to a high consumption of Portland cement. It is estimated that cement production corresponds to about 4-10% of the global CO_2 emissions, mostly produced within the combustion processes involved in cement calcination [1-2]. Due to the critical environmental impact of cement production, considerable efforts have been devoted to the design of alternative materials with the potential to replace common cementitious materials.

A promising alternative is the group of geopolymers, characterized by a low carbon footprint under certain conditions and comparable or even better material properties [3]. These inorganic materials with repeating (polymeric) structures are formed by the activation of amorphous calcium aluminosilicates (precursors) by alkali activators, which are usually potassium or sodium silicates (water glass), hydroxides, or by combinations of these two compounds. The precursors are typically secondary raw materials or waste substances from industrial production (slag, fly ash, waste metakaolin or metashale, brick powder, etc.), thus, the origin and local availability of input geopolymer materials favorably influence the financial demands and low ecological burden of geopolymer production [4-6].

* Corresponding author. E-mail address: petr.hotek@fsv.cvut.cz

English language proofreader: Yen-Chun Hsieh

With the increasing demands of the construction industry on building materials, there is a growing interest in designing multifunctional or so-called smart materials. Due to new material properties, these materials offer entirely new application potential and can take new roles in structural elements. Most of these new capabilities, such as self-sensing, self-heating, energy harvesting, or electromagnetic shielding/absorbing are strongly dependent on the electrical and thermal material parameters [7].

Therefore, electrically conductive admixtures (ECA) are added to the fresh mixture within the production of multifunctional mortars or concretes. The main reasons are increasing the effective electrical conductivity, optimizing AC electrical properties, or adjusting the thermo- and piezoelectric properties of the material, resulting in well-formed conductive paths or appropriate ECA distribution in the material matrix. The particular ECA amount ensuring the requested function varies according to the type and level of expected electrical properties. There are several types of ECAs in the form of powder, fibers, or tubes, with the most commonly used carbonaceous admixtures such as graphite powder (GP), carbon black (CB), carbon fibers (CF), carbon nanofibers (CNFs), carbon nanotubes (CNT), multiwalled carbon nanotubes (MWCNT), or graphene nanoplatelets (GNPs) [8-10]. In general, carbonaceous materials are beneficial due to higher electrical conductivity and chemical stability compared to metallic admixtures which can be passivated at high pH of fresh mixtures.

The self-sensing building materials have the potential to early detect defects in structures or monitor applied forces and corresponding deformations, respectively. Electrical properties of materials optimized with ECAs, such as DC resistance/resistivity and conductance/conductivity, or AC resistance or capacitance are proportional to a current compressive force load. Emerging cracks or a decrease in the applied force are revealed by increased electrical resistance. On the contrary, an increase in the force is accompanied by decreased resistance due to the approaching of electrically conductive elements in the aluminosilicate matrix. The material sensitivity is expressed by the fractional change in resistivity (FCR) which is evaluated for the data obtained by a dynamic loading.

This approach was used by Dong et al. [11], who designed a self-sensing cement-based sensor for human motion and vehicle passing detection that was tested through dynamic loading under compressive loading in real conditions. Guo et al. [12] verified the self-sensing performance of cement-based sensors with CB and polypropylene fibers subjected to different loading conditions, comparing the effect of fibers and their surface treatment on the results of self-sensing tests. Electrical properties of materials (even with an optimized amount of ECA for reliable stress/strain sensing) are also influenced by temperature and moisture content [13]. Therefore, in practical applications on construction sites, these effects should be compensated by processing, and data analyzing systems [14].

The paper is focused on the design of new geopolymer mortars based on alkali-activated metashale calcined clay. The electrical properties of the mortars were optimized by doping with particle-based GP and fibrous CF which was also supposed to enhance mechanical properties and avoid crack propagation [15]. The self-sensing capability of mixtures with GP/CF ratios of 5/0, 4.5/0.5, 4/1 (in the total 5 wt.% of ECAs amount), and 3/0 is expressed through the FCR indicator evaluated from the dynamic compressive loading tests and corresponding DC electric response. Besides, the common material properties, such as basic physical, mechanical, thermal, and electrical properties were determined to get a complex insight into the applicability in civil engineering.

2. Experimental

In the Experimental part of the paper, the properties of the raw materials used in the production of the geopolymer composite were specified in more detail. Furthermore, the procedure for the production of the samples in each step was described and the methods of all measurements used in the characterization of the material properties were presented. materials used in the production of the geopolymer composite.

2.1. Materials

The set of multifunctional composites was designed based on the Mefisto L05 aluminosilicate precursor, as shown in Fig. 1(a), which is produced by thermal and granulometric processing of clays and floating kaolins by České lupkové závody a.s. This precursor is rich in alumina and silica content (see Table 1, Al_2O_3 – 47.3%, SiO_2 – 49.1%) and consists of fine particles defined by the specific surface area of 12690 $m^2 \cdot kg^{-1}$, and d_{50} = 3 μm / d_{90} = 10 μm. Alkali activation was conducted by a combination of potassium water glass (K_2SiO_3) with Ka_2O/SiO_2 ratio = 1.7 and potassium hydroxide in the form of small white flakes. The filler was represented by 3 quartz sand fractions PGI 0.08-0.5 mm, PGII 0.5-1 mm, and PGIII 1-2 mm. The ECAs admixed to fresh mortars were represented by GP (Fig. 1(b)) and CF (Fig. 1(c)). The powder of the GP spherical particles was characterized by d_{50} = 8.76 μm and d_{90} = 19.72 μm.

(a) Metashale Mefisto L05 (b) Graphite powder (c) Carbon fibers

Fig. 1 Carbonaceous electrically conductive admixtures

Table 1 Composition of Mefisto L05 (XRF analysis)

Component	CaO	Al_2O_3	MgO	SiO_2	Fe_2O_3	TiO_2	K_2O
Component content	0.9	41.04	1.08	49.58	2.76	2.39	1.03

2.2. Samples preparation

Multifunctional geopolymer mortars with GP and CFs were prepared according to the following procedure: The metashale Mefisto L05 was first mixed with PGI, PGII, and PGIII fractions of quartz. In the next step, a graphite suspension was prepared as follows: GP was poured into a container, and water was added along with the siloxane-based air-detraining agent Lukosan S and non-ionic surfactant Triton X-100 to defoam the suspension and reduce the surface tension of GP particles. The required dispersion of the GP particles in water was achieved by mechanical mixing of the suspension with IKA ULTRA-TURRAX high-speed homogenizer for 10 minutes followed by ultrasonic mixing of the vessel content in a bath for an additional 5 minutes. The homogenized suspension was then mixed with the precursor, quartz sand, and a mix of potassium water glass and hydroxide activator was added. All components were properly stirred by a standard stirrer for 5 minutes and then the CFs were gradually added into the fresh mortar within the continuing 5 minutes of mixing.

The fresh mortars were placed into (100 × 100 × 100) mm^3 molds for further determination of electrical properties and self-sensing capability and (160 × 40 × 40) mm^3 for the determination of basic physical and mechanical properties, as shown in Fig. 2(a). Copper grid electrodes were placed into (100 × 100 × 100) mm^3 fresh samples in two arrangements. The samples embedded with 2 electrodes (Fig. 2(b)) were used for DC and AC electrical characterization whereas those embedded with 4 electrodes were used in self-sensing capability tests (Fig. 2(c)). All the samples were finally demolded after 24 h and cured in the laboratory conditions (22 °C, 50% RH) to simulate real conditions. The composition of the designed mixtures, referred to as metashale graphite fibers (MGF), is summarized in Table 2.

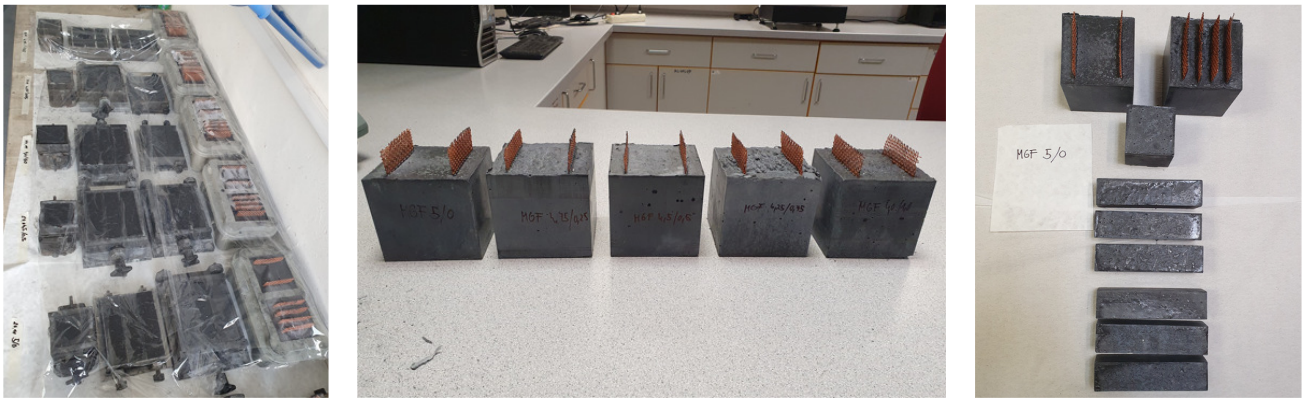

(a) Moulded fresh mixtures (b) Samples with 2 embedded electrodes (c) Set of MGF 5/0 samples

Fig. 2 Samples for material characterization

Table 2 Composition of the geopolymer mortars

Component (g)	MGF 5/0	MGF 4.5/0.5	MGF 4/1	MGF 3/0
Mefisto L05	1920	1920	1920	1920
K_2SiO_3	669	669	669	669
KOH	72	72	72	72
PGI (0.08-0.5 mm)	2400	2400	2400	2400
PGII (0.5-1 mm)	1200	1200	1200	1200
PGIII (1-2 mm)	1440	1440	1440	1440
Carbon fibers	0	35	69	0
Graphite powder	348	313	279	209
Water	812	732	650	490

2.3. *Basic physical, mechanical, thermal, and electrical properties*

The bulk and matrix density ρ_v (kg·m^{-3}) and ρ_{mat} (kg·m^{-3}) were determined on samples of (160 × 40 × 40) mm^3 by the gravimetric method, and small pieces of samples (approximately 10 g) using helium pycnometry (Pycnomatic ATC EVO device), respectively. The total open porosity ψ (%) was then calculated using the mass m (kg), volume V (m^3), and the matrix density ρ_{mat} (kg·m^{-3}) of the samples according to the following equations:

$$\rho_v = \frac{m}{V} \tag{1}$$

$$\psi = \left(1 - \frac{\rho_v}{\rho_{mat}}\right) \times 100 \tag{2}$$

Mechanical properties of the mortars (compressive and flexural strengths) were carried out at 28 days according to ČSN EN 196-1 [16] on 3 samples with dimensions (160 × 40 × 40) mm^3 using mechanical and hydraulic presses FP100 and ED60, respectively. Thermal properties were determined on (100 × 100 × 100) mm^3 samples by ISOMET 2114 device with an attached surface probe. The non-steady state method based on material response to the generated heat pulses (heat-pulse method) provided the thermal conductivity, volumetric heat capacity, and thermal diffusivity values. Electrical characterization of the mortars involved DC and AC electrical measurements on (100 × 100 × 100) mm^3 samples with 2 embedded electrodes through which the material was connected to the measuring instruments.

The measurements of the volt-ampere characteristic (electrical voltage and corresponding current values) were performed by GW Instek GPR-11H30D power source and two Fluke 8846A multimeters in the range of 0-100 V with 10 V steps. Based on the results, the electrical resistance R (Ω) and electrical conductivity σ (S·m^{-1}) of the material were evaluated for different voltage levels as described in:

$$\sigma = \frac{I}{U} \times \frac{l}{S} = \frac{1}{R} \times \frac{l}{S} \tag{3}$$

where I (A) is the electric current, U (V) is the voltage, $S = 0.0072$ (m^2) is the area of the electrodes, $l = 0.07$ (m) is the distance between the electrodes, and R (Ω) is the resistance of the material.

AC electrical parameters were represented by the magnitude of the impedance Z (Ω) and the phase shift Θ (°). Measurements were performed (100 × 100 × 100) mm^3 samples with 2 embedded electrodes using the GW Instek 8210 LCR bridge in the range of 10 Hz – 10 MHz.

2.4. *Self-sensing experiment*

The self-sensing capability was tested on (100 × 100 × 100) mm^3 samples with 4 embedded electrodes. Such an arrangement was used to partially reduce the effect of polarization, which is limiting for the 2-probe arrangement. The pair of outer electrodes was used for circuit-supplying whereas the inner ones monitored changes of the sample resistance caused by applied compressive force.

Particular samples were dynamically loaded with a defined compressive force perpendicular to the direction of the copper electrodes (Fig. 3(a)). The experiment consisted of 5 cyclic loadings to the maximum of 10 kN and successive unloadings with a linear loading/unloading rate of 300 N.s^{-1}. The maximum loading force was chosen to be less than 10% of the materials' compressive strengths to ensure elastic behavior. Electrical response (electrical voltage) corresponding to mechanical loadings was logged by the DEWE-5000 device (Fig. 3(b)). The electric circuit (Fig. 3(c)) represented by the voltage divider consisted of a DC power source (21.34 V) connected in series to the sample (resistance R_1 (Ω) changing during the loading/unloading) and inserted constant resistance R_2 (Ω) of the defined value (R_2 was chosen based on the resistance of unloaded material samples to identify the current I (A) passing through R_1 and R_2).

(a) Self-sensing experimental setup

(b) DEWE-5000 datalogger

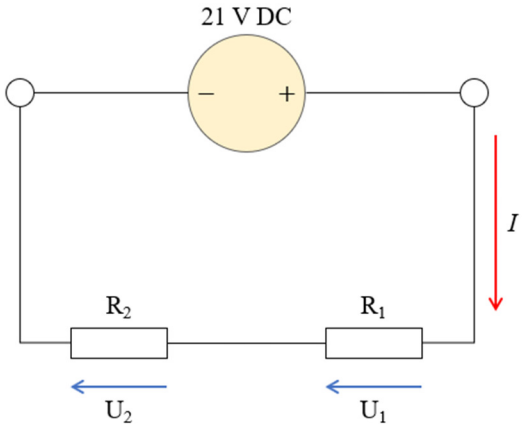

(c) Measuring electric circuit

Fig. 3 Arrangement of the self-sensing experiment

The power source was pinned up to the sample's outer electrodes whereas the sensing was read out from the sample's inner electrodes to avoid polarization effects. The actual sample's resistance R_1 (Ω) was calculated using the logged voltage (U_1) and passing current I.

$$U_1 = U \times \frac{R_1}{R_1 + R_2} \tag{4}$$

$$U_2 = U \times \frac{R_2}{R_1 + R_2} \tag{5}$$

where R_1 (Ω) is the electrical resistance of the sample, R_2 (Ω) is the additional constant resistance, U (V) is the voltage of the DC power supply, U_1 (V) is the voltage of the sample, and U_2 (V) is the voltage on the resistor. The sensitivity of the material is expressed by the FCR (%) and was calculated according to

$$FCR = \frac{R_1 - R_{1,unloaded}}{R_{1,unloaded}} \times 100 \quad (6)$$

where R_1 (Ω) is the actual resistance during the loading/unloading, and $R_{1,unloaded}$ (Ω) is the electrical resistance of the unloaded sample.

3. Results and Discussion

In the following section of the presented work, the results of the basic physical, mechanical thermal and electrical properties as well as images showing the results of the self-sensing experiment were presented and discussed. In each section, the values obtained from individual measurements were presented and compared with the results of other authors working on the same topic.

3.1. Basic physical properties

In Table 3, basic physical properties represented by the bulk density, the matrix density, and the total open porosity are summarized. The highest bulk density was expected of the MGF 3/0 (1994 kg·m^{-3}) mixture that contained the lowest amount of GP and was without CFs. The decreasing tendency was observed for increasing amounts of GP and CFs and the lowest value exhibited MGF 4/1 (1759 kg·m^{-3}). The matrix density ranged from 2418-2515 kg·m^{-3} and did not exhibit a significant change with increasing amounts of ECAs, pointing to similar densities of GP and CFs. Total open porosity was lowest for MGF 3/0 (17.54%) and systematically increased with increasing ECA and especially with increasing CF amount up to 29.62% for MGF 4/1.

The changes in physical properties were mainly observed for the samples with higher CF amounts which corresponds to imperfect dispersion of CF in the material matrix. The decreasing trend in bulk density and the increase in total open porosity therefore indicate a correlation. Fiala et al. [17] in their paper studied the basic physical properties of alkali-activated aluminosilicates with CB admixture and observed the same trends in bulk density while maintaining the matrix density. The increase in porosity in CF-doped composites was presented also by Zhang et al. [18], who observed an increase in capillary porosity with increasing CF content in the material matrix.

Table 3 Basic physical properties of the studied mortars

Properties	MGF 5/0	MGF 4.5/0.5	MGF 4/1	MGF 3/0
Bulk density (kg·m^{-3})	1873	1872	1759	1994
Matrix density (kg·m^{-3})	2515	2512	2500	2418
Total open porosity (%)	25.53	25.50	29.62	17.54

3.2. Mechanical properties

In Fig. 4 and Fig. 5, the mechanical properties represented by compressive and flexural strengths after 28 days of aging are introduced. The highest compressive strength value was determined for MGF 3/0 (34.24 MPa) and continued to decrease with increasing ECA to the lowest value of MGF 5/0 (10.11 MPa). A slight increase was observed for MGF 4.5/0.5 (13.29 MPa) and MGF 4/1 (13.44 MPa), which is due to the presence of CF. The same trend was observed for the flexural strength, the highest value of MGF 3/0 (3.07 MPa) and the lowest value of MGF 5/0 (1.97 MPa) were observed. The higher strength of materials with CFs (MGF 4.5/0.5 and MGF 4/1) compared to the MGF 5/0 (carbonaceous admixtures in total were equal to 5

wt.%) were due to better reinforcing behavior of fibers than of spherical particles dispersed in calcium aluminosilicate matrix. In general, mechanical properties were in good agreement with basic physical properties, and their decrease was systematically observed with increasing amounts of ECA.

Cheng et al. [19] reported in the study dealing with the electrical resistance and self-sealing properties of pressure-sensitive materials with graphite filler in Kuralon fiber concrete described a trend identical to the statement presented in this paper. For mixtures with GP content (0-16 %), a decrease in compressive strength as the ECA content increased from approximately 42.5 to 32.5 MPa. Similar behavior was introduced for the flexural strength, where a decrease from 6.5 to 5 MPa was observed. A similar trend was also reported by Garcés et al. [20] who dealt with the determination of mechanical properties and corrosion of calcium aluminate cement (CAC) mortars with carbon fiber admixture (0-5%). The specimen with 0.5% CF exhibited higher compressive strength compared to the reference mortar. However, a further CF content increase led to a decrease in the compressive strength.

Comprehensive results were presented by Zhang et al. [21] who reported mechanical properties for geopolymer composites with CF admixture from 0 to 1% with 0.2% step. The results indicated an increasing tendency of both tensile and flexural strength up to CF content of 0.6% (35.7 and 5.9 MPa), and further the mechanical performance decreased with increasing content of ECA up to 32.2 and 5.2 MPa for 1% CF, which indicated a certain percolation threshold.

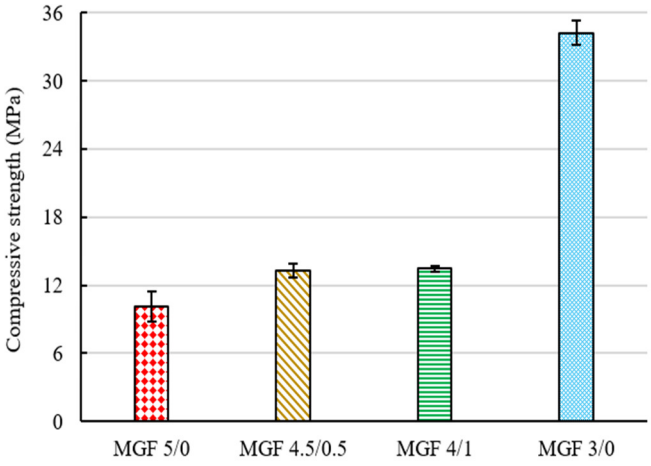

Fig. 4 28d compressive strength of the studied mortars

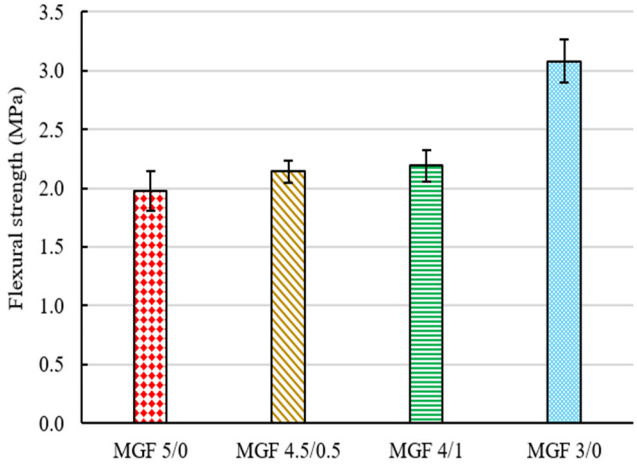

Fig. 5 28d flexural strength of the studied mortars

3.3. Thermal and electrical properties

The thermal properties of mortars represented by the thermal conductivity and specific heat capacity are summarized in Table 4. The thermal conductivity ranged from 0.93 to 1.06 $W \cdot m^{-1} \cdot K^{-1}$ and did not show significant changes. The highest thermal conductivity exhibited MGF 4/1 (1.06 $W \cdot m^{-1} \cdot K^{-1}$). The specific heat capacity ranged from 788 to 950 $J \cdot kg^{-1} \cdot K^{-1}$. The highest value was observed for MGF 4/1 (950 $J \cdot kg^{-1} \cdot K^{-1}$) whereas the lowest for MGF 5/0 (788 $J \cdot kg^{-1} \cdot K^{-1}$). The specific heat capacity was highest for the samples with CFs and increased with increasing CF content.

DC electrical properties represented by the electrical conductivity/electrical resistance are presented in Table 4. The highest electrical conductivity exhibited MGF 4/1 ($8.7 \cdot 10^{-1}$ $S \cdot m^{-1}$) whereas the lowest was observed for MGF 3/0 ($2.2 \cdot 10^{-6}$ $S \cdot m^{-1}$). It was confirmed an increasing trend with an increasing amount of ECA with a dominant increase caused by CFs. It is therefore obvious that despite the constant total amount of ECAs (5% in MGF 5/0, MGF 4.5/0.5, and MGF 4/1), CFs easily form conductive paths due to favorable fibrous shape.

The same trend of a positive influence of CFs on an increase in electrical conductivity was reported by Luo et al. [22] who reported electrical conductivity of 10^{-1} $S \cdot m^{-1}$ for 0.5% CF, which was higher than for the reported MGF 4.5/0.5 also containing 4.5% GP. Such a discrepancy in results can be explained by different compositions of the mixtures and types of

CFs. Gomis et al. [23] compared the electrical resistance of cement pastes doped with different ECAs. The paste with 5% GP reached 1100 Ω which is comparable to MGF 5/0 (1300 Ω). Considering the aggregates involved in the MGF 5/0 composite that are preventing the formation of conductive paths, better dispersion of GP in the MGF's matrix is indicated by the observed favorable resistance.

Table 4 Thermal and DC electrical properties of studied mortars

Properties	MGF 5/0	MGF 4.5/0.5	MGF 4/1	MGF 3/0
Thermal conductivity ($W \cdot m^{-1} \cdot K^{-1}$)	0.98	1.04	1.06	0.93
Specific heat capacity ($J \cdot kg^{-1} \cdot K^{-1}$)	788	888	950	790
Electrical conductivity ($S \cdot m^{-1}$)	$9.7 \cdot 10^{-3}$	$8.4 \cdot 10^{-2}$	$8.7 \cdot 10^{-1}$	$2.2 \cdot 10^{-6}$
Electrical resistance (Ω)	1300	1100	146	9950000

AC electrical properties represented by the magnitude of the impedance and the phase shift in the frequency range of 10 Hz-10 MHz are summarized in Fig. 6. MGF 3/0 showed an unstable waveform with high fluctuation of the magnitude of the impedance, the highest values of the magnitude of the impedance around $7 \cdot 10^8$ Ω which indicates capacitive behavior (data for MGF 3/0 are not included in Fig. 6(a) for better readability). The magnitude of the impedance of the rest of the MGF mortars systematically decreased with increasing frequency. The lowest difference in values in the whole frequency range was observed for MGF 5/0. The mortars with CFs exhibited similar frequency-dependent behavior. The dependence of the phase shift dependence on the frequency (Fig. 6(b)) confirmed the rather capacitive nature of MGF 3/0 which is typical by curve fluctuations at low frequencies and values far from 0° (ideal resistor – self-heating potential), closer to -90° (ideal capacitor). The phase shift curves of MGF mixtures with 5 wt.% of GP and CFs in the total were similar and exhibited rather resistive behavior.

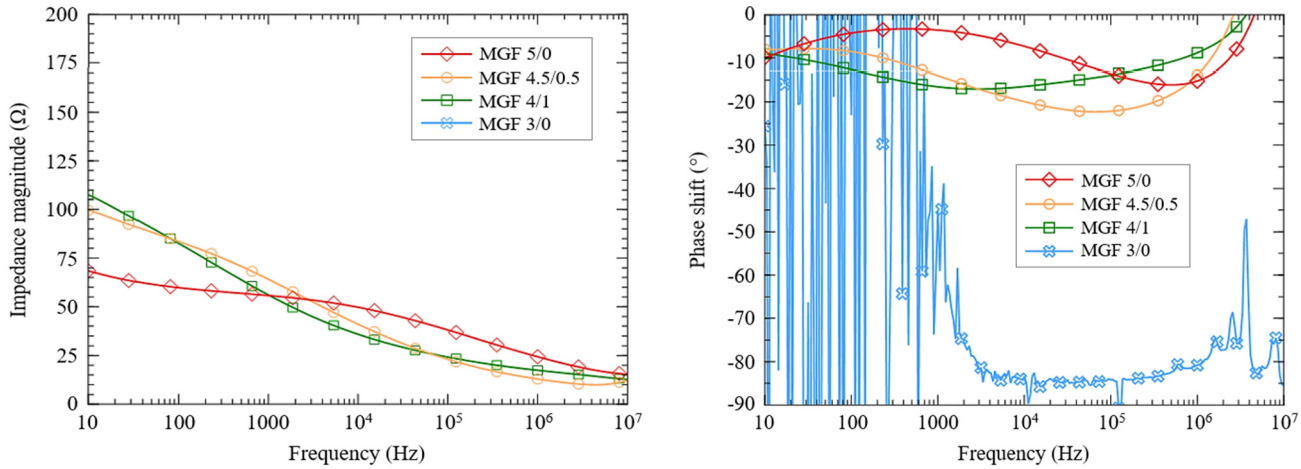

(a) Magnitude of the impedance (b) Phase shift

Fig. 6 AC characterization of the studied mortars

3.4. *Self-sensing capability*

FCR was calculated according to Eq. (6) using the data from the conducted self-sensing experiments (5 loading cycles, maximum compressive force of 10 kN applied to the area of (100 × 100) mm^2 which corresponds to 1 MPa stress). In Fig. 7(a) and Fig. 7(b), results of the self-sensing experiments for mixtures with just spherical GP admixture (MGF 5/0 and MGF 3/0) are presented. MGF 5/0 exhibited increasing absolute values of FCR during the dynamic loading with a maximum value of -0.013% after 5 cycles. This trend can be caused by plastic deformations that remained after the loading stage (GP particles in the matrix remain closer). On the contrary, MGF 3/0 was defined by the maximum absolute value of FCR (0.0032%) at the first cycle of loading of the material. The sensitivity was lower mainly due to lower maximum loading stress to the compressive strength (34.24 MPa) ratio. The opposite trend of MGF 5/0 can be explained by the higher distance between particles and the dominant effect of electrode polarization. MGF 3/0 reached its minimum FCR (0.0043%) at the 5th cycle.

The dynamic sensing properties of multifunctional cementitious composites doped with CB powder (similar to GP) have been further described by Monteiro et al. [24]. In their article, they presented an analogous dynamic loading setup with a maximum load of 20 kN. The FCR results ranged from 0 to ±0.004%, which were lower FCR values compared to those presented in this study. According to Rovnaník et al. [25], the decrease in electrical resistivity during unloading was caused by the healing of micro-cracks and defects caused by dry shrinkage, while the increase in resistivity was justified by the gravity defect. Rovnaník et al. [26] further studied the self-sensing capability of composites with GP admixture in the amount of 0, 5, and 10%. The best AC sensing performance at 1 kHz was observed for 10% of GP with the highest load sensitivity (FCR = 17%) at 50 kN. In the paper, the author further determined that in the DC measurements, the experimental results were greatly influenced by the strong polarization of the electrodes, resulting in an independence of sensitivity to the amount of ECA applied.

The self-sensing ability of MGF 4.5/0.5 and MGF 4/1 which contain both, GP and CF admixtures, is presented in Fig. 7(c) and Fig. 7(d). Promising results were observed for MGF 4.5/0.5. The course of the electrical response was similar to that of MGF 3/0, but higher sensing ability was achieved. The maximum FCR value (-0.019%) was reached within the first loading cycle. MGF 4/1 exhibited a decreasing trend in the absolute value of FCR with the maximum in the first cycle of loading (-0.0125%). The FCR curve was scattered, with a high level of electrical noise, and the electrical response was delayed relative to the mechanical loading. It showed that MGF 4/1 mortar exhibited the worst sensing ability.

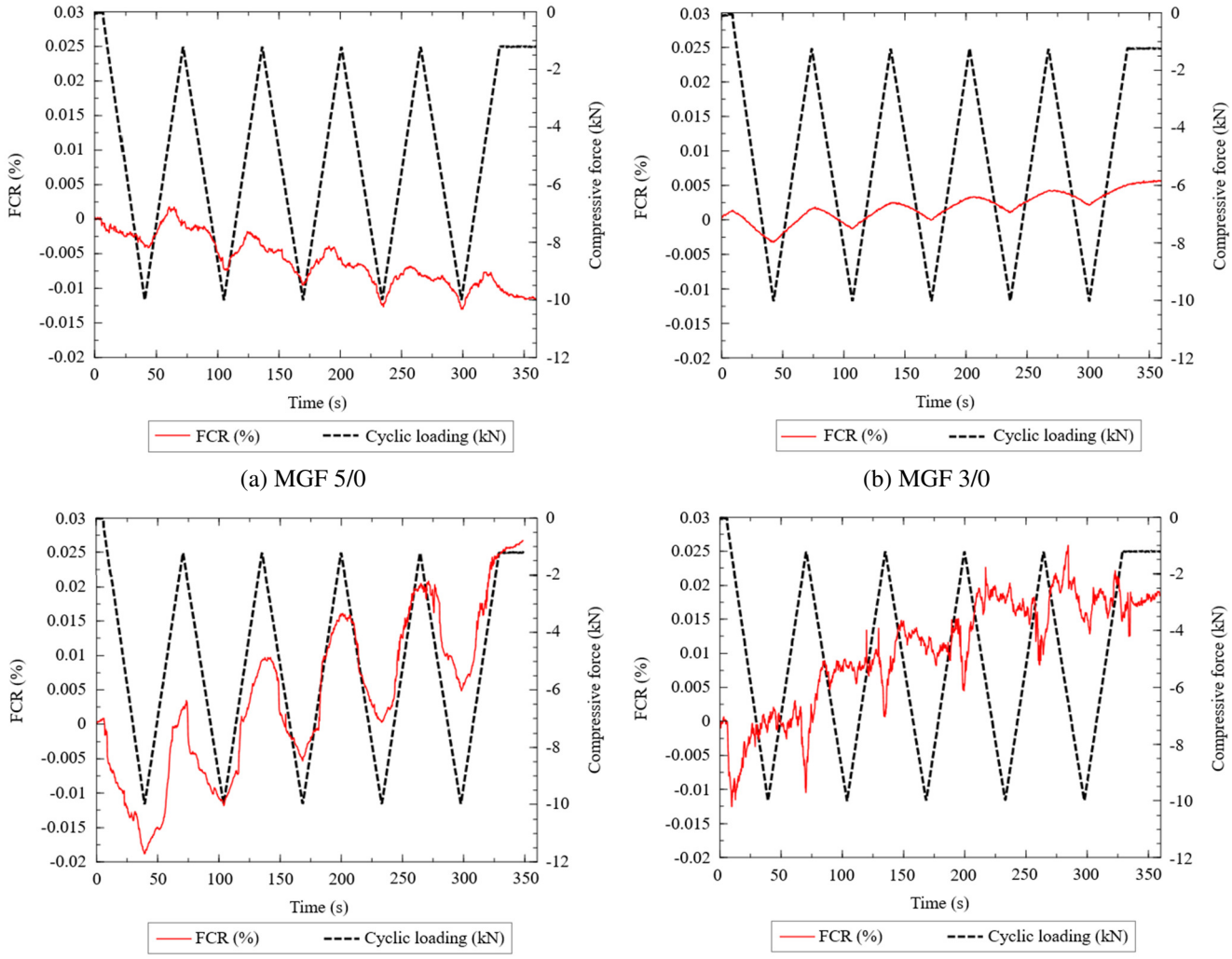

(a) MGF 5/0 (b) MGF 3/0

(c) MGF 4.5/0.5 (d) MGF 4/1

Fig. 7 Electrical response of the studied mortars to dynamic cyclic loading

Azhari and Banthia [27] studied cement-based sensors with a CF content of 15% in a 100 kHz AC regime. They observed the maximum FCR (-0.5%) under the 70 kN load which was of significantly higher sensitivity to loading compared to the samples investigated in this research. Nevertheless, it should be mentioned that the compressive force was higher and the AC

measuring regime was used (compared to the 10 kN and DC regime presented in this research). Ma et al. [28] published a paper on the self-sensing ability of materials based on different types of precursors with 0.3% carbon fiber admixture. They applied loads in the range of 0-3.25 MPa (5.2 kN) and 0-25 MPa (40 kN) during dynamic loading of the specimen. They observed very similar results of material response to loading cycles in the range of 0 to -0.015% (ΔR-R_0). Chung [29] justified our observations concerning the unstable self-sensing behavior of materials with higher contents of CFs and concluded that the reduced self-sensing efficiency was caused by small spaces (pores) between CF clusters (not well-dispersed CFs in the material matrix).

4. Conclusions

The paper was focused on the design, comprehensive material characterization, and evaluation of the self-sensing potential of metashale geopolymer mortars with different ratios of CF and GP admixtures. The material characterization involved the determination of the basic physical, mechanical, thermal, and DC/AC electrical properties. It was observed that the mechanical properties are significantly dependent on the amount of ECAs. With the increasing amount of ECA, both the compressive and flexural strengths decreased, which was associated with the porosity increase. The increase in porosity was subsequently justified in the discussion by the increased amount of pores caused, mainly by fiber clustering. It was confirmed that higher amounts of GP/CFs resulted in the electrical conductivity increase (electrical resistivity decrease), but negatively influenced the electrical response (noise, delay).

Despite the known limitations of DC sensing arrangement and application of lower compressive force (10 kN) on the studied mortars, the self-sensing capability was observed for all the mixtures. The most promising results were achieved for MGF 5/0, although the highest FCR values were determined for MGF 4.5/0.5 mixture (-0.019%). The tested materials did not exhibit a constant base resistance level ensuring long-term sensing repeatability which is typically due to electrode polarization effect. Therefore, further testing in the AC electrical field will be performed.

Acknowledgments

The research has been supported by the Czech Science Foundation under the project No. 22-00987J.

Conflicts of Interest

The authors declare no conflict of interest.

References

[1] F. Farooq, X. Jin, M. F. Javed, A. Akbar, M. I. Shah, F. Aslam, et al., "Geopolymer Concrete as Sustainable Material: A State of the Art Review," Construction and Building Materials, vol. 306, article no. 124762, November 2021.

[2] H. van Oss and A. C. Padovani, "Cement Manufacture and the Environment Part II: Environmental Challenges and Opportunities," Journal of Industrial Ecology, vol. 7, no. 1, pp. 93-126, January 2003.

[3] A. Ślosarczyk, J. Fořt, I. Klapiszewska, M. Thomas, Ł. Klapiszewski, and R. Černý, "A Literature Review of the Latest Trends and Perspectives regarding Alkali-Activated Materials in Terms of Sustainable Development," Journal of Materials Research and Technology, vol. 25, pp. 5394-5425, July–August 2023.

[4] Y. Li, J. Shen, H. Lin, and Y. Li, "Optimization Design for Alkali-Activated Slag-Fly Ash Geopolymer Concrete Based on Artificial Intelligence considering Compressive Strength, Cost, and Carbon Emission," Journal of Building Engineering, vol. 75, article no. 106929, September 2023.

[5] J. Li, B. W. Y. Tay, J. Lei, and E. H. Yang, "Experimental Investigation of Seebeck Effect in Metakaolin-Based Geopolymer," Construction and Building Materials, vol. 272, article no. 121615, February 2021.

[6] J. Fořt and R. Černý, "Transition to Circular Economy in the Construction Industry: Environmental Aspects of Waste Brick Recycling Scenarios," Waste Management, vol. 118, pp. 510-520, December 2020.

[7] B. Han, S. Sun, S. Ding, L. Zhang, X. Yu, and J. Ou, "Review of Nanocarbon-Engineered Multifunctional Cementitious Composites," Composites Part A: Applied Science and Manufacturing, vol. 70, pp. 69-81, March 2015.
[8] L. Fiala, V. Pommer, M. Böhm, L. Scheinherrová, and R. Černý, "Self-Heating Alkali Activated Materials: Microstructure and Its Effect on Electrical, Thermal and Mechanical Properties," Construction and Building Materials, vol. 335, article no. 127527, June 2022.
[9] S. Gwon, H. Kim, and M. Shin, "Self-Heating Characteristics of Electrically Conductive Cement Composites with Carbon Black and Carbon Fiber," Cement and Concrete Composites, vol. 137, article no. 104942, March 2023.
[10] S. Rana, P. Subramani, R. Fangueiro, and A. G. Correia, "A Review on Smart Self-Sensing Composite Materials for Civil Engineering Applications," AIMS Materials Science, vol. 3, no. 2, pp. 357-379, 2016.
[11] W. Dong, W. Li, Y. Guo, Z. Sun, F. Qu, R. Liang, et al., "Application of Intrinsic Self-Sensing Cement-Based Sensor for Traffic Detection of Human Motion and Vehicle Speed," Construction and Building Materials, vol. 355, article no. 129130, November 2022.
[12] Y. Guo, W. Li, W. Dong, Z. Luo, F. Qu, F. Yang, et al., "Self-Sensing Performance of Cement-Based Sensor with Carbon Black and Polypropylene Fibre Subjected to Different Loading Conditions," Journal of Building Engineering, vol. 59, article no.105003, November 2022.
[13] S. Ding, S. Dong, A. Ashour, and B. Han, "Development of Sensing Concrete: Principles, Properties and Its Applications," Journal of Applied Physics, vol. 126, no. 24, article no. 241101, December 2019.
[14] Z. Tian, Y. Li, J. Zheng, and S. Wang, "A State-of-the-Art on Self-Sensing Concrete: Materials, Fabrication and Properties," Composites Part B: Engineering, vol. 177, article no. 107437, November 2019.
[15] V. Růžek, A. M. Dostayeva, J. Walter, T. Grab, and K. Korniejenko, "Carbon Fiber-Reinforced Geopolymer Composites: A Review," Fibers, vol. 11, no. 2, article no. 17, February 2023.
[16] Methods of Testing Cement - Part 1: Determination of Strength, ČSN EN 196-1 (722100) Standard, 2016.
[17] L. Fiala, M. Jerman, P. Rovnanik, and R. Černý, "Basic Physical, Mechanical and Electrical Properties of Electrically Enhanced Alkali-Activated Aluminosilicates," Materiali in Tehnologije/Materials and Technology, vol. 51, no. 6, pp. 1005-1009, 2017.
[18] J. Zhang, A. Heath, R. J. Ball, and K. Paine, "Effect of Fibre Loading on the Microstructural, Electrical, and Mechanical Properties of Carbon Fibre Incorporated Smart Cement-Based Composites," Frontiers in Materials, vol. 9, article no. 1055796, November 2022.
[19] A. Cheng, W. T. Lin, L. Fiala, P. Hotěk, S. J. Chao, and H. M. Hsu, "Electrical Resistance and Self-Sensing Properties of Pressure-Sensitive Materials with Graphite Filler in Kuralon Fiber Concrete," Materials Science-Poland, vol. 40, no. 2, pp. 223-239, August 2022.
[20] P. Garcés, E. Zornoza, E. G. Alcocel, Ó. Galao, and L. G. Andión, "Mechanical Properties and Corrosion of CAC Mortars with Carbon Fibers," Construction and Building Materials, vol. 34, pp. 91-96, September 2012.
[21] D. Zhang, Y. Wang, T. Zhang, and Q. Yang, "Engineering and Microstructural Properties of Carbon-Fiber-Reinforced Fly-Ash-Based Geopolymer Composites," Journal of Building Engineering, vol. 79, article no. 107883, November 2023.
[22] T. Luo, H. Yuan, and Q. Wang, "Comparison the Properties of Carbon Fiber-Based Portland Cement and Alkali-Activated Fly Ash/Slag Conductive Cementitious Composites," Journal of Building Engineering, vol. 76, article no. 107134, October 2023.
[23] J. Gomis, O. Galao, V. Gomis, E. Zornoza, and P. Garcés, "Self-Heating and Deicing Conductive Cement. Experimental Study and Modeling," Construction and Building Materials, vol. 75, pp. 442-449, January 2015.
[24] A. O. Monteiro, P. M. F. J. Costa, M. Oeser, and P. B. Cachim, "Dynamic Sensing Properties of a Multifunctional Cement Composite with Carbon Black for Traffic Monitoring," Smart Materials and Structures, vol. 29, no. 2, article no. 025023, February 2020.
[25] P. Rovnaník, I. Kusák, P. Bayer, P. Schmid, and L. Fiala, "Comparison of Electrical and Self-Sensing Properties of Portland Cement and Alkali-Activated Slag Mortars," Cement and Concrete Research, vol. 118, pp. 84-91, April 2019.
[26] P. Rovnaník, I. Kusák, P. Bayer, P. Schmid, and L. Fiala, "Electrical and Self-Sensing Properties of Alkali-Activated Slag Composite with Graphite Filler," Materials, vol. 12, no. 10, article no.1616, May 2019.
[27] F. Azhari and N. Banthia, "Cement-Based Sensors with Carbon Fibers and Carbon Nanotubes for Piezoresistive Sensing," Cement and Concrete Composites, vol. 34, no. 7, pp. 866-873, August 2012.
[28] Y. Ma, F. Li, H. Xie, W. Liu, X. Ouyang, J. Fu, et al., "Self-Sensing Properties of Alkali-Activated Materials Prepared with Different Precursors," Construction and Building Materials, vol. 409, article no. 134201, December 2023.
[29] D. D. L. Chung, "A Critical Review of Electrical-Resistance-Based Self-Sensing in Conductive Cement-Based Materials," Carbon, vol. 203, pp. 311-325, January 2023.